A 4.5 Year-Long Record of Svalbard Water Vapor Isotopic Composition Documents Winter Air Mass Origin

C. Leroy-Dos Santos[1], V. Masson-Delmotte[1], M. Casado[2], E. Fourré[1], H. C. Steen-Larsen[3], M. Maturilli[4], A. Orsi[1], A. Berchet[1], O. Cattani[1], B. Minster[1], J. Gherardi[1], and A. Landais[1]

[1]Laboratoire des Sciences du Climat et de l'Environnement, UMR CEA-CNRS-UVSQ/IPSL, Gif-sur-Yvette, France, [2]Alfred Wegener Institute Helmholtz-Center for Polar and Marine Research Bremerhaven, Bremerhaven, Germany, [3]Geophysical Institute, University of Bergen, Bergen, Norway, [4]Alfred Wegener Institute Helmholtz-Center for Polar and Marine Research, Potsdam, Germany

Abstract From May 2014 to September 2018, a laser spectrometer analyzer provided a 4.5 years continuous record of water vapor isotopic composition at Ny-Ålesund (8 m above sea level, a.s.l.), Svalbard. It corresponds to the longest data set published in polar regions. A comparison of this data set with a parallel similar data set obtained during 20 days by a second laser spectrometer installed near Mount Zeppelin (474 m a.s.l.) shows that this data set is representative of a regional signal. In addition, the observation of insignificant diurnal cycles in the isotopic signal compared to the strong isotopic signature of synoptic events and the comparison of simultaneous measurements in the vapor and in rain or snow samples lead to the conclusion that our record reflects a large part of the regional dynamics of the atmospheric water cycle driven by large-scale variability. This study focuses on winters dominated by the occurrence of synoptic events associated with humidity peaks. Using statistics and back trajectories calculations, we link high humidity peaks characterized by an anticorrelation between $\delta^{18}O$ and d-excess in the water vapor to a rapid shift of air mass source regions from the Arctic to the North Atlantic Ocean below 60°N. On the other hand, correlation between $\delta^{18}O$ and d-excess may be associated with a shift of air mass sources within the Arctic. These results demonstrate the added value of long-term water vapor isotopic monitoring to better understand the moisture origin in the Arctic and the atmospheric dynamics.

1. Introduction

In the current context of climate change, the Arctic region is specifically under focus because of the extreme high temperatures and low sea ice extents observed over recent years (Arctic Monitoring and Assessment Programme, 2017; Meredith et al., 2019; Overland & Wang, 2018; Walsh et al., 2017). The long-term increase in annual temperature in the Arctic region is 2–3 times larger than the global average (Gjelten et al., 2016), due to a number of polar amplification processes involving changes in albedo, water vapor, summer cloudiness, the presence of open water in autumn, and also the transport of heat and moisture associated with the intrusion of subarctic storms (Goosse et al., 2018; Meredith et al., 2019; Screen & Simmonds, 2010). Linked to atmospheric circulation patterns, recent studies also highlighted the occurrence of "atmospheric rivers" as an important modulation of the moisture transport to the Arctic region (Alekseev et al., 2019; Bonne et al., 2015; Hao et al., 2019; Liu & Barnes, 2015; Naakka et al., 2019; Woods et al., 2013).

Seasonally surrounded by sea ice, Svalbard stands at the intersection between cold polar air traveling from the north and oceanic air traveling from the south (Figure 1). Svalbard is hence at a key location to study changes of the atmospheric water cycle organization in the Arctic region, which is key to gain a better understanding of the role of sea ice extent variations on the Arctic climate processes (Ding et al., 2017) since recent sea ice decline leads to an increase of local evaporation sources (Dufour et al., 2016). Due to its geographic position, Svalbard climate evolution is strongly affected by Arctic amplification (warming at a rate of 0.8 $\pm$ 0.2°C decade^{-1} on the 1979–2019 period (Figure S1 and Text S1 in the supporting information) and is influenced by regional processes controlling sea ice variations and moisture transport from the North Atlantic sector (Dahlke et al., 2020; Hanssen-Bauer & Førland, 1998; Isaksen et al., 2016; Rinke et al., 2017).
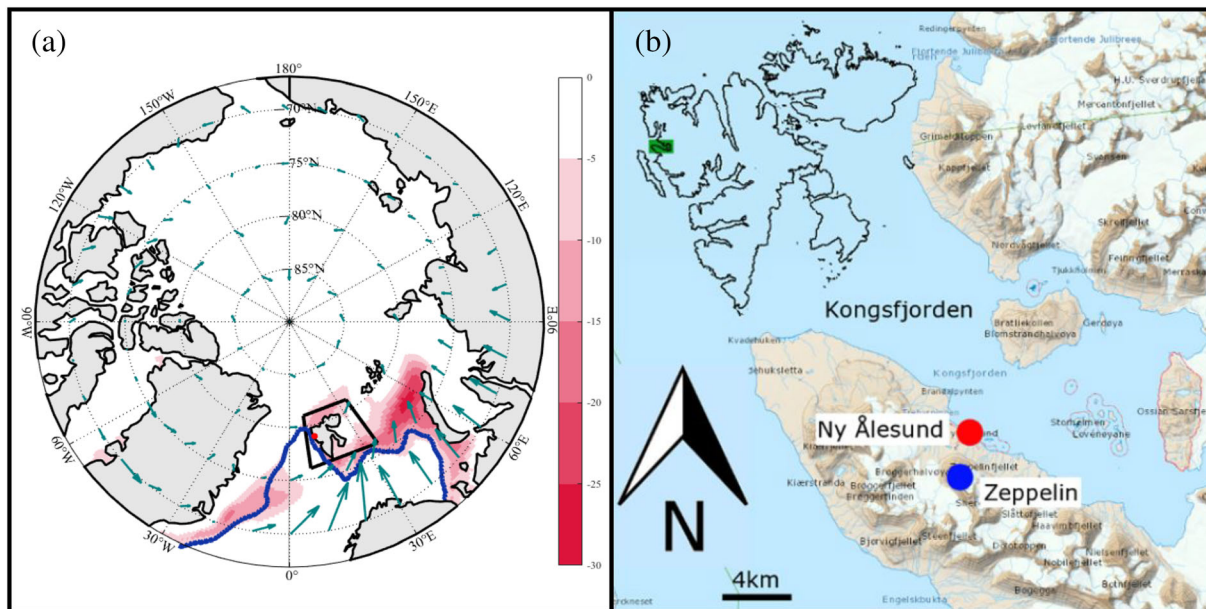
Figure 1. (a) Linear trend (% per decade) of winter maximum sea ice concentration from ERA-5 reanalyses (over the 1979–2018 period) in pink; mean-sea ice extent in March (blue line); integrated horizontal vapor fluxes (DJF) are plotted on some grid points (green arrow lengths are proportional to vapor flux in kg m^{-1} s^{-1}). The area delineated by the black line corresponds to ERA 5 selected grid points used in supporting information Figure S1. (b) Map of Kongsfjorden, Svalbard (modified from Eckhardt et al., 2013): Ny-Ålesund (8 m a.s.l.) and Zeppelin (474 m a.s.l.).

A robust signal in climate projections is the increasing trend of Arctic precipitation by the end of the 21st century, but climate models show a large dispersion in the relative contributions of local recycling and enhanced advection to this increase in precipitation amount (Bintanja & Selten, 2014). Two main effects are expected to influence the moisture content in the Svalbard region: evaporation over the ocean (Dufour et al., 2016) and atmospheric circulation patterns leading to moisture transport from Atlantic, Arctic, or continental regions (Dahlke & Maturilli, 2017; Vázquez et al., 2016). This motivates the exploration of the air mass origin signal captured by water stable isotopes in Svalbard water vapor and precipitation in this study.

Water stable isotopes are a classical tool to study the organization of the atmospheric water cycle (Gat, 1996; Jouzel, 2003). We use the δ notation to express the ratio (in per mil, ‰) between heavier (HD^{16}O or H$_2$^{18}O) molecules and lighter molecules (H$_2$^{16}O): δ = ($R_{\text{sample}}/R_{\text{VSMOW}}$ − 1) * 1,000 where R_{sample} is the ratio between heavier and lighter water molecules of measured sample and R_{VSMOW} is the ratio between heavier and lighter water molecules of the reference water (Vienna Standard Mean Ocean Water). In polar continental regions such as Greenland or the East Antarctic plateau, δ^{18}O and δD are closely controlled by changes in temperature along the trajectory from the warm regions of evaporation to the polar regions leading to a distillation process and thus a decrease in the heavy isotope content in atmospheric water vapor (Jouzel et al., 2013; Masson-Delmotte et al., 2008). In addition, the second-order parameter, d-excess (d-excess = δD – 8 * δ^{18}O, Dansgaard, 1964) brings complementary information on the climatic conditions of the source evaporative region and moisture recycling over the distillation path. Variations in d-excess result from different sensitivities of δD and δ^{18}O to kinetic fractionation processes such as diffusion during evaporation and moisture uptake occurring along the atmospheric transport pathway (Craig & Gordon, 1965). During evaporation over the ocean, high (low) relative humidity levels lead to small (high) kinetic fractionation hence low (high) d-excess. The combination of δ^{18}O and δD can thus provide quantitative insights on the origin and dynamics of moisture trajectories. Bonne et al. (2014) have shown that this initial d-excess signal is partially preserved during moisture transport toward Greenland. During snow formation, kinetic effects are also at play, especially for situation of high supersaturation, and they affect the d-excess values in polar regions (Jouzel & Merlivat, 1984).

Until recently, water isotopes measurements were only possible on the condensed phase, hence limiting their use to the study of atmospheric water cycle of rain and snowfall events. Some early studies performed water

vapor analyses by trapping water vapor in a cold trap for several hours to get sufficient water for liquid analyses (Angert et al., 2004; Steen-Larsen et al., 2011). The recent progress of optical spectroscopy now permits the continuous measurement with high accuracy of the water vapor isotopic composition (Aemisegger et al., 2012; Galewsky et al., 2016; Tremoy et al., 2011). This new ability to monitor continuously δD and δ18O of the water vapor has been implemented during several measurement campaigns in different Arctic environments: over the Greenland ice sheet in summer (Berkelhammer et al., 2016; Steen-Larsen et al., 2013, 2014), in the marine boundary layer during oceanic campaigns on research vessels (Benetti et al., 2017; Bonne et al., 2019), as at coastal sites (Bonne et al., 2014; Kopec et al., 2014; Steen-Larsen et al., 2015), or in more continental and vegetated area like Siberia (Bastrikov et al., 2014). While being very useful to characterize the water cycle dynamics over a period in the region of interest, there are some limitations in the series already available. For example, none of the aforementioned records exceeds 12 consecutive months of monitoring at the same place, while at least 24 months would be needed to study interannual variations of the vapor isotopic composition.

With the aim to study the changes of origin of moisture trajectories to the Arctic region and the link with synoptic variability at seasonal and interannual scales, we installed a laser spectroscopy instrument to monitor the evolution of δ18O and δD at Ny-Ålesund AWIPEV station, Svalbard (8 m above sea level, a.s.l., Figure 1). It results in the longest time series record of water vapor stable isotopic composition (4.5 years), a period characterized by the highest mean annual temperature over the 1979–2018 period (−1.1°C in 2016) and by a low sea ice extent, as shown in Figure S1. This record has been completed with a comparison to measurements of water vapor isotopic composition at the neighbor site of Mount Zeppelin (474 m a.s.l.). Additionally, meteoric water samples were recovered at Ny-Ålesund AWIPEV station during each precipitation event, rainfall or snowfall.

This paper is organized into three sections. In section 2, we present the methods used to obtain, calibrate, and validate the 4.5-year records of water isotopic composition in vapor and in precipitation, as well as meteorological data at the study site and methods to retrieve 5-day back trajectories. Section 3 presents the full data set. Section 4 focuses on the information brought by water isotopes to document the origin of moisture arriving to Svalbard during winter humidity peaks.

2. Data and Methods

2.1. Meteorological Data

Meteorological data are available since 1993 at the AWIPEV observatory (Maturilli, 2020a). Hereafter, we use the 2-m air temperature (°C), the specific humidity (volume mixing ratio in ppmv), the cloud base (CLB) height (m) (Maturilli & Ebell, 2018), and the radiosonde measurements (Maturilli, 2018, 2020b) from Ny-Ålesund station provided by the Alfred Wegener Institute-Research Unit Potsdam.

We also use outputs from the global atmospheric reanalysis of the European Center for Medium-Range Weather Forecasts (ECMWF), ERA-5 6-hourly averaged data on pressure levels from 1979 to 2018: the total daily precipitation amount (m), the sea ice area fraction, the vertical integral of the water vapor flux (kg m^{-1} s^{-1}) and the temperature (°C).

2.2. Water Vapor Monitoring

Two Picarro laser spectrometer instruments based on the cavity ring-down spectroscopy (CRDS) technique were installed in Ny-Ålesund (8 m a.s.l.), in the AWIPEV observatory building (Figure S3; Text S3): a L1102-i Picarro instrument from May 2014 to May 2015 and then a L2130-i Picarro instrument until the end of the measurement campaign (27 September 2018). The change of instrument is justified by the enhanced performances of the more recent L2130-i Picarro (precision of 0.1‰ and 0.8‰ for δ18O and δD, respectively, 30-s injection at 2,500 ppmv, measurement rate of 1 Hz) compared to the L1102-i Picarro (precision of 0.2‰ and 1‰ for δ18O and δD, respectively, 30-s injection at 10,000 ppmv, measurement rate of 0.1 Hz) (Picarro Inc., 2009, 2016). The outside air was continuously pumped through a heated sampling line installed along the building, with an inlet located 10 m above the ground level. The instrumental transition occurred in two phases: first, the L2130-i instrument was installed at Zeppelin observatory (474 m a.s.l., 1.2 km from Ny-Ålesund) and operated in parallel with the L1102-i instrument at Ny-Ålesund during 2 weeks (6–23 May 2015, Figure S4). It was then set up at Ny-Ålesund (8 m a.s.l.) to replace the L1102-i instrument. The full
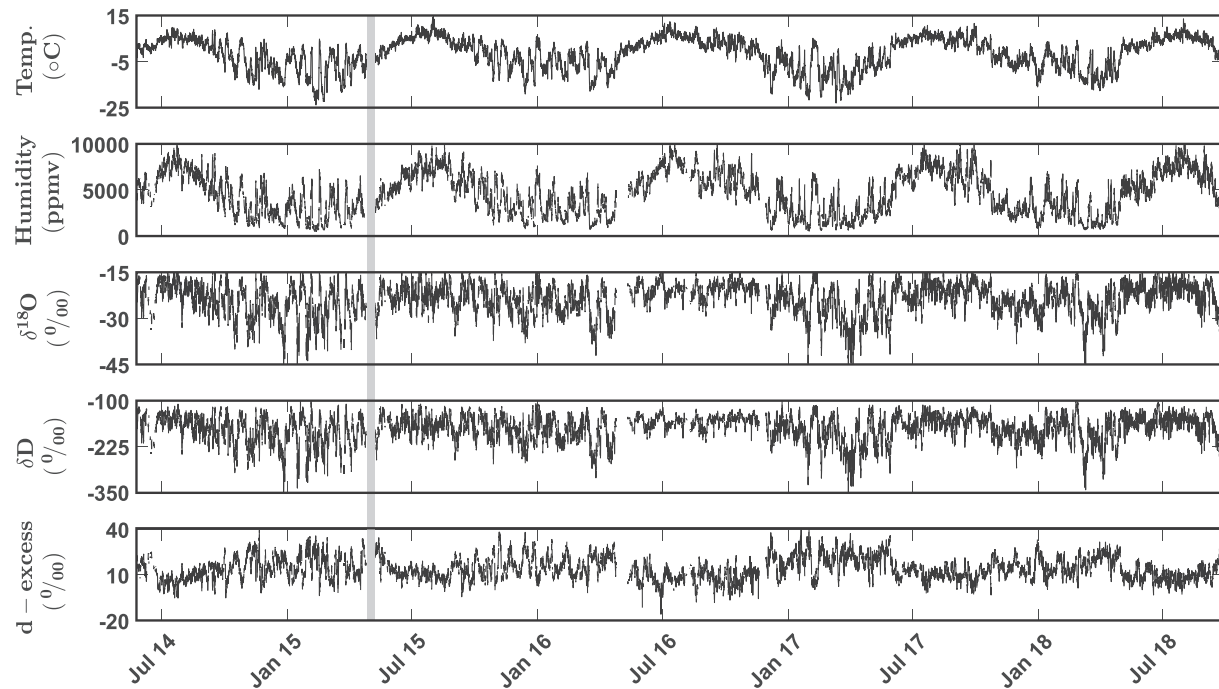
Figure 2. From top to bottom: temperature, humidity, $\delta^{18}O$, δD, and d-excess of atmospheric water vapor at 10 m. The full data series (black) was corrected following the calibration procedure described in Texts S5, S6, and S7 in the supporting information and show clear seasonal variations. The gray period corresponds to the switch of instrument (from L1102-i to L2130-i). Note that different correction factors were implemented for the first instrument and the second one.

data series at Ny-Ålesund (Figure 2) presents some missing measurements: (1) every day, 2 hr were dedicated to standard measurements for calibration; (2) some longer periods (e.g., from 23 April 2016 to 11 May 2016) were dedicated to the maintenance of the setup.

The raw data from the CRDS instruments need to be calibrated as discussed previously in several publications to ensure consistency with the international VSMOW-SLAP scale (International Atomic Energy Agency, 2006). The volume water vapor mixing ratio in ppmv, hereafter referred to as humidity, is continuously measured by the CRDS instrument. A multiplying correction factor (0.91 and 1.02, respectively, for our L1102-i and L2130-i instruments) is applied to the measured humidity in order to match the local meteorological data from AWIPEV (Figure S5 and Texts S4 and S5).

Following the protocol outlined in previous publications (Bonne et al., 2014; Steen-Larsen et al., 2014; Tremoy et al., 2011), three main corrections are applied to the isotopic data to account for the following: (1) the influence of humidity on $\delta^{18}O$ and δD measurement (Text S6), (2) the shift between the measured values and the true isotopic values (Text S7), and (3) the temporal drift of the instrument (Text S7), which refers to the temporal evolution of the shift between measured and true values (Figure S6). The calibration setup introduces vapor into the instrument with a known isotopic composition at prescribed humidity levels (Text S4). The influence of humidity on water vapor isotopic composition is determined during two calibration campaigns through a series of measurements of water isotopic standard injected at different humidity levels (Figure S7).

The isotope-humidity calibration determined for the second instrument is unfortunately more scattered than that for the first instrument below 2,000 ppmv. It nevertheless shows that, above 2,000 ppmv, the isotope versus humidity correction is small (<0.1‰ and <0.3‰ for $\delta^{18}O$ and δD, respectively). The mean standard deviation is 1.3‰ (6.5‰) for $\delta^{18}O$ (δD) for measurements performed at humidity levels lower than 2,000 ppmv and 0.4‰ (1.4‰) for $\delta^{18}O$ (δD) measurement performed at humidity levels higher than 2,000 ppmv (Text S6 and Figures S6 and S7). This study will thus focus on winter periods during which humidity values are higher than 2,000 ppmv.

The other two corrections are calculated by measuring two water isotopic standards with isotopic values bracketing the measured values at least once a day at constant humidity level (set at 3700 ppmv between May 2014 and December 2016 and then at 6900 ppmv for the rest of the campaign) (Texts S4, S7, and Figure S6). The uncertainty on the water vapor isotopic data can then be calculated from the instrument replication (internal accuracy) and the uncertainties associated with these corrections (Text S8, Figures S8, S9, and S10).

When the calibration system is working adequately (79% of the time), the uncertainty only due to the reproducibility of daily standard measurements (including internal accuracy and uncertainty on the drift of the instrument) is estimated to 0.11 ‰ for $\delta^{18}O$ and 0.70 ‰ for δD. When no daily calibration is available (21% of the time), this uncertainty rises up to 0.18 ‰ for $\delta^{18}O$ and 1.38 ‰ for δD. This uncertainty does not take into account possible biases due to variation of the influence of humidity on water vapor isotopic composition which is expected to be constant over the whole period of measurements according to our measurements (Text S6 and Figure S7) and previous study (Bailey et al., 2015).

2.3. Precipitation Monitoring

Whenever precipitation events occurred, water or snow was sampled daily at midday and stored in a glass container at 8–10 °C and shipped to LSCE for measurement. Altogether, 519 samples were collected over the 4.5 years. Samples were sent back to LSCE every 6 months. Water stable isotope measurements were performed with a Picarro CRDS instrument working in liquid mode, i.e. with vaporization of the samples in dry air to reach a humidity of 20,000 ppmv. Replicates were performed over 15% of the samples so that we could calculate the uncertainty (2σ) for our data set to 0.05 ‰ and 0.2 ‰ respectively for $\delta^{18}O$ and δD.

2.4. Back Trajectories

The origin and trajectory of air masses were evaluated using the HYSPLIT model (Hybrid-Single Particle Lagrangian Integrated Trajectory) (Stein et al., 2015; http://ready.arl.noaa.gov/HYSPLIT_traj.php). In this model, the position of the air mass is determined using a three-dimensional Lagrangian air mass vertical velocity algorithm. The set of meteorological data used to simulate trajectories was taken from ERA-5. We have calculated 5 days back trajectories with a single launch of one particle every 6 hours at 500 m a.s.l. above Ny-Ålesund coordinates throughout the full data series period. Hysplit was used here to provide an estimate of the origin of air masses over specific moist events from our 4.5 years' data set. We have chosen a 500 m a.s.l altitude for the particle launch for several reasons. First, the vertical mixing in HYSPLIT is not ideally represented (Ngan et al., 2019) so that we expect artifacts when running the particle launch at 10 m a.s.l. (where the inlet was actually located). Second, we checked that the temporal evolution of the water vapor isotopic composition is the same at 10 m a.s.l. and 500 m a.s.l. (section 3.4). Finally, a sensitivity test has been performed comparing back trajectories at 500 and 10 m a.s.l. on a 2-year period (June 2014 to September 2016): only 20 back trajectories over 308 have opposite origin when comparing those obtained from a launch of particles at 500 m a.s.l. to those obtained from a launch of particles at 10 m a.s.l. Despite being convenient to produce diagnostics over long time series, Hysplit has however some limitations. As Hysplit computations are based on single-particle trajectories, the representativeness of our estimates might not be correct. To assess this point, we used in addition to Hysplit the Lagrangian Particle Dispersion Model Flexpart (Stohl et al., 2005) with a large ensemble of particles for a couple of selected events: every 6 hr a batch of 500 neutral inert air tracer particles are randomly released from a volume ($0.1° \times 0.1° \times 100$ m) centered around Ny-Ålesund coordinates (at an altitude of 50 m a.s.l.). Flexpart is driven by meteorological fields from ERA5 to compute 10-day back trajectories. We developed visualization tools to display the concentration of particles being transported above each grid point in latitude-longitude and latitude-altitude maps (Text S9).

3. Results

In this section, we first present the full 4.5-year data set at Ny-Ålesund for the water vapor isotopic composition as well as its variability at the interannual, seasonal, and diurnal scale. This data set is then compared to the short series of parallel measurements of the water vapor at the nearby site of Mount Zeppelin (474 m a.s.l.), and finally to the 4.5 years' record of meteoric water isotopic composition sampled at the event scale at Ny-Ålesund.
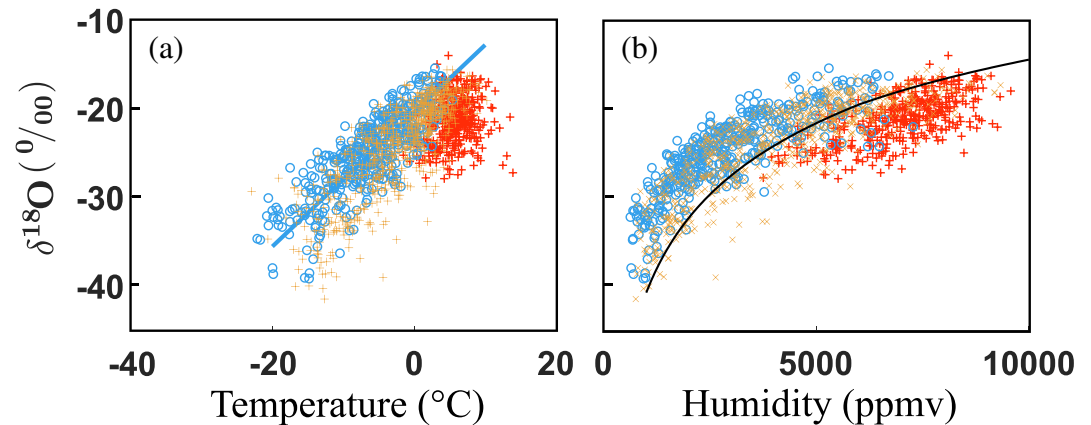
Figure 3. Observed relationship between surface water vapor $\delta^{18}O$ and surface air temperature (a) and between surface water vapor $\delta^{18}O$ and humidity (b). The colors of data points vary according to the seasons: blue circles for winter (DJF), yellow crosses for autumn (SON) and spring (MAM), red crosses for summer (JJA) seasons. The blue line in Figure 3a is the linear fit between $\delta^{18}O$ and temperature during winter (DJF), the black line in Figure 3b) is the model output from MCIM (Mixed Cloud Isotopic Model, Ciais & Jouzel, 1994, initial conditions: surface pressure = 1,015 hPa, surface temperature = 290 K and surface relative humidity = 80%).

3.1. Isotopic Composition of the Vapor Water at Ny-Ålesund and Links With Meteorological Data

The full calibrated hourly data series spanning 4.5 years are displayed in Figure 2.

Our data set depicts a clear covariance in temperature, humidity, and water vapor $\delta^{18}O$. On the contrary, we observe a global anticorrelation between d-excess and $\delta^{18}O$ ($R = -0.68$) or δD. The $\delta^{18}O$ versus temperature slope over the full record (Figure 3a) is 0.62‰.°C^{-1} for the entire series (0.78‰.°C^{-1} when considering only winter, i.e., DJF). This relationship between water vapor $\delta^{18}O$ and temperature lies within previous estimates in the region. The temporal slope observed at the coastal Greenland site of Ivittuut is smaller (0.37‰.°C^{-1}, Bonne et al., 2014) and such a low value could be linked to the latitude of Ivittuut, lower than at Ny-Ålesund. Over the northwest Greenland ice sheet, the isotopic record of the NEEM station spans summer only and is marked by strong diurnal cycles probably associated with local exchanges between snow surface and water vapor superimposed on the synoptic signal (Steen-Larsen et al., 2013). The NEEM data set spanning three consecutive summer seasons is associated with a temporal slope of 1.1‰.°C^{-1}, that is, almost twice larger than the $\delta^{18}O$ versus temperature slope of our record.

The observed relationship between humidity and water vapor $\delta^{18}O$ is displayed in Figure 3b. The general pattern is very close to the theoretical relationship between water vapor $\delta^{18}O$ and humidity predicted by a Rayleigh distillation along a trajectory starting from evaporation over the midlatitude ocean (see black line in Figure 3b). The relatively low water vapor $\delta^{18}O$ values (-40 to $-15‰$) indicate that the recharge of water vapor by local ocean evaporation is small at least during winter. Indeed, the isotopic composition of water vapor evaporating over the open ocean in North Atlantic is about $-8‰$ to $-20‰$ (Benetti et al., 2017, 2018; Bonne et al., 2019; Steen-Larsen et al., 2015, 2017) so that a strong recharge would lead to higher $\delta^{18}O$ values than observed in winter. In summer, the relatively high values of $\delta^{18}O$ values of water vapor can be due to some local evaporation. The results obtained here suggest that the variability of the $\delta^{18}O$ signal in winter is driven by different degrees of distillation of advected air masses (Dansgaard, 1964; Rayleigh, 1902) in addition to a switch of distant moisture sources (Vázquez et al., 2016).

3.2. Seasonal and Diurnal Variabilities

Seasonal variations are observed unequivocally in both temperature and humidity (Table 1) which reach maximum values in summer, respectively, 5.0°C and 6,900 ppm, and minimum values in winter, respectively, -7.0°C and 2,800 ppm (average values over JJA and DJF, respectively, over the whole time period). Similarly, higher values are observed in summer for water vapor isotopic composition (+4.1‰ and +25.5‰ in average for $\delta^{18}O$ and δD, respectively, compared to winter values), as expected from the

Table 1
Mean and Standard Deviation of Meteorogical Parameters and Isotopic Composition Calculated From Hourly Means

Year	Summer (JJA)						Winter (DJF)		
	Hum (ppmv)	RH (%)	T (°C)	δ^{18}O (‰)	δ D (‰)	d-xs (‰)	Hum (ppmv)	RH (%)	T (°C)
14	**6,800** $\pm$ 1,200	**82** $\pm$ 9	**3.9** $\pm$ 2.3	**−20.9** $\pm$ 3.2	**−158.7** $\pm$ 21.9	**8.4** $\pm$ 5.4	**2,400** $\pm$ 1,400	**65** $\pm$ 12	**−9.1** $\pm$ 6.3
15	**6,900** $\pm$ 1,200	**76** $\pm$ 11	**5.7** $\pm$ 2.4	**−22.1** $\pm$ 3.2	**−166.0** $\pm$ 22.7	**10.6** $\pm$ 3.6	**3,000** $\pm$ 1,400	**69** $\pm$ 11	**−5.7** $\pm$ 4.9
16	**7,000** $\pm$ 1,300	**77** $\pm$ 11	**5.4** $\pm$ 2.4	**−21.1** $\pm$ 3.0	**−160.8** $\pm$ 16	**8.3** $\pm$ 5.4	**2,700** $\pm$ 1700	**67** $\pm$ 14	**−8.2** $\pm$ 6.2
17	**6,900** $\pm$ 1,100	**79** $\pm$ 9	**4.7** $\pm$ 2	**−21.0** $\pm$ 3.1	**−157.0** $\pm$ 21.3	**11.0** $\pm$ 4	**3,100** $\pm$ 1,300	**66** $\pm$ 12	**−4.9** $\pm$ 4.1
18	**7,000** $\pm$ 1,300	**78** $\pm$ 9	**5.1** $\pm$ 2.1	**−20.7** $\pm$ 3.1	**−156.9** $\pm$ 21.7	**8.9** $\pm$ 4.4	//	//	//
TOT	**6,900** $\pm$ 1,200	**79** $\pm$ 10	**5.0** $\pm$ 2.3	**−21.2** $\pm$ 3.1	**−159.9** $\pm$ 21.2	**9.5** $\pm$ 4.7	**2,800** $\pm$ 1,500	**68** $\pm$ 12	**−7.0** $\pm$ 5.7

Note. Total standard deviation is calculated from the concatenated seasons at hourly resolution. Summer 14 corresponds to JJA of year 2014 and winter 14 corresponds to December 2014, January 2015, and February 2015.

temperature-to-isotopic composition relationship. The d-excess signal depicts lower values in summer than in winter, hence in anticorrelation with δ^{18}O. This result is similar to observations by Bonne et al. (2014) in South Greenland but opposite to the d-excess maximum observed in summer precipitation in central Greenland (Kopec et al., 2019).

The intraseasonal variability is much larger in winter than in summer: the winter standard deviation is almost twice larger for temperature, δ^{18}O and δD compared to summer. The humidity and d-excess variability is also larger in winter than in summer. The strong winter variability motivates us to explore the associated mechanisms and their potential links to synoptic scale events.

In contrast with results of water vapor time series from sites marked by large diurnal variations in local boundary layer winds or evapotranspiration (Berkelhammer et al., 2016; Bréant et al., 2019; Kopec et al., 2014; Steen-Larsen et al., 2013), diurnal variations are very small in our record, with diurnal amplitudes of temperature, humidity or δ^{18}O variations below 2°C, 870 ppm, and 3.2‰, respectively, independently of the season. In our data set, the mean diurnal variations have values comparable to the lowest diurnal variability observed in polar sites marked by large boundary layer variations (Bréant et al., 2019). This implies that our record is moderately influenced by diurnal changes in local surface fluxes and boundary layer mixing. This supports the finding that the Svalbard surface water vapor isotopic composition does not bear a clear signature of exchange with the local oceanic surface on diurnal time scales.

3.3. Comparison Between Sea Level AWIPEV and 474 m a.s.l. Zeppelin Observatory Isotopic Vapor Data

During 2 weeks, in May 2015, water vapor isotopic composition was measured at two sites in parallel (Figure S4). A very high correlation is observed between the two data sets ($R > 0.9$ for humidity and δ^{18}O, $R = 0.8$ for d-excess), with only a slight offset for humidity (average mixing ratio of 4,000 and 3,900 ppmv for AWIPEV station and Mount Zeppelin, respectively), and for the mean δ^{18}O (−24.0‰ and −23.3‰ for AWIPEV station and Mount Zeppelin, respectively). Temperatures at both sites are well correlated ($R = 0.87$) during this period, but show an average difference of −3°C between Mount Zeppelin and AWIPEV. The high correlation between the two temperature records agrees with the high covariance between both isotopic signals but cannot explain why the offset between the two δ^{18}O series is smaller than expected from the temperature versus δ^{18}O slope determined in section 3.1. A better explanation for this small shift is probably to be found in calibration issues with the Mount Zeppelin instrument (Figure S7). In the following discussion, we mainly focus on the water isotopic variability, and our findings are not challenged by this offset.

The strong correlation between the vapor isotopic composition measurement data sets near the surface and at 474 m a.s.l. justifies the assumption that the variations of the water vapor isotopic signal at Ny-Ålesund reflect the dynamics of the lower troposphere moisture isotopic composition driven by large scale regional variability, and not local boundary layer dynamics or sources. This finding is also supported by the analysis of almost 20 years of radiosondes measurements in Svalbard (Maturilli & Kayser, 2017), showing that local

Table 1
Continued

| Year | Winter (DJF) | | | Full year (Jan to Dec) | | | | | |
	δ^{18}O (‰)	δ D (‰)	d-xs (‰)	Hum (ppmv)	RH (%)	T (°C)	δ^{18}O (‰)	δ D (‰)	d-xs (‰)
14	**−27.2** ± 6.2	**−199.6** ± 46.3	**17.6** ± 7.3	//	//	//	//	//	//
15	**−25.0** ± 4.3	**−183.9** ± 32.2	**16.5** ± 6.9	4,200 ± 2,200	72 ± 12	**−2.1** ± 7.1	**−24.0** ± 5.0	**−177.2** ± 36.0	**14.9** ± 7.5
16	**−25.0** ± 4.9	**−180.7** ± 35.4	**19.3** ± 7.9	4,900 ± 2,200	73.5 ± 12	**−0.8** ± 6.1	**−22.5** ± 4.3	**−168.1** ± 30	**12.2** ± 7.4
17	**−24.0** ± 4.0	**−177.8** ± 30.9	**14.5** ± 5.9	4,200 ± 2,400	70 ± 12	**−2.7** ± 7.3	**−24.5** ± 5.5	**−180.1** ± 38.9	**15.9** ± 7.5
18	//	//	//	//	//	//	//	//	//
TOT	**−25.3** ± 5.1	**−185.4** ± 37.6	**17.0** ± 7.3	4,600 ± 2,300	72 ± 12	**−1.6** ± 6.7	**−23.6** ± 5.1	**−175.0** ± 36.1	**14.0** ± 7.4

Note. Total standard deviation is calculated from the concatenated seasons at hourly resolution. Summer 14 corresponds to JJA of year 2014 and winter 14 corresponds to December 2014, January 2015, and February 2015.

boundary layer characteristics are directly influenced by large scale dynamics such as Arctic Oscillation changes, even in winter time when an inner fjord weather regime can superimpose.

3.4. Comparison Between Vapor and Precipitation Isotopic Composition

The full data series of the isotopic composition of precipitation together with surface air temperature measurements during precipitation days is presented in the supporting information (Text S10 and Figure S11). The average δ^{18}O and d-excess over the measurement period are −9.6 ± 4.6‰ and 6.2 ± 10.5‰ with significant seasonal variations. The variability is twice larger during winter than during summer for δ^{18}O, as already observed for the vapor isotopic composition (Table 1). This is mainly due to the large range of temperature variations in winter compared to summer (factor of 2 between both variabilities).

The precipitation δ^{18}O values observed at Ny-Ålesund are coherent with the precipitation δ^{18}O values in the Arctic region as documented by the IAEA/WMO Global Network for Isotopes in Precipitation (GNIP) database with monthly δ^{18}O values varying between −9‰ and −17‰ in North Sweden. In Ivittuut (Greenland), Bonne et al. (2014) also found similar δ^{18}O values for precipitation between −5‰ and −20‰. Svalbard ice core δ^{18}O variations from Isaksson et al. (2005) show a range of more depleted δ^{18}O values (around −16‰ to −17‰), which are consistent with a stronger distillation toward higher altitudes (drilling altitude of ice cores of 1,250 and 750 m, respectively) than for a coastal site such as Ny-Ålesund (Smith & Evans, 2007; Stern & Blisniuk, 2002).

In order to compare the precipitation isotopic signal to the vapor signal, we calculated the theoretical isotopic composition of a vapor at equilibrium with each precipitation sample. Equilibrium fractionation coefficients are temperature-dependent and it is not obvious to define which equilibrium temperature should be used within the atmospheric column between the cloud base (where precipitation forms) and surface temperature (where liquid precipitation can be reequilibrated with the surrounding water vapor measured by the Picarro instrument). Several sensitivity tests were performed (Text S10 and Figure S12) and equilibrium fractionation coefficients were finally computed with 2-m air temperature for rain samples (because of possible exchange with water vapor at this sampling height), and with cloud base height temperature for solid precipitation. Indeed, we assumed that the isotopic composition of snow does not significantly change during its descent and possible partial sublimation along the atmospheric column (Maturilli & Kayser, 2017). For our calculation, we used liquid-vapor and solid-vapor fractionation coefficients at equilibrium from Majoube (1971) and Merlivat and Nief (1967).

Figures 4 and S13 show the reconstructed water vapor δ^{18}O series calculated from precipitations (see also Figures S12 and S13) along with the δ^{18}O directly measured in the vapor. Both δ^{18}O series share around 60% of variance ($R = 0.78$). Such a good correlation shows that synoptic events affecting the water vapor isotopic composition should also be recorded in the snow and rain when these synoptic events are associated with precipitation. The remaining unexplained variance can be due to kinetic effects occurring (1) during precipitation reevaporation within the atmospheric column or most probably during the 24-hr period between precipitation and sampling, (2) during precipitation formation in supersaturation condition or mixed-phase clouds.
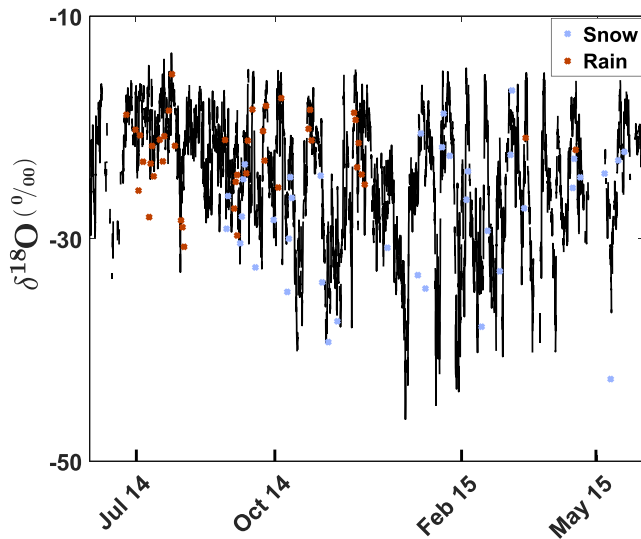
Figure 4. Comparison over 1 year (from 1 June 2014 to 1 June 2015) of the $\delta^{18}O$ measured in the vapor (black line, hourly averaged) and the theoretical computed $\delta^{18}O$ of vapor in equilibrium with precipitation samples collected daily at AWIPEV station (light blue for snow and red for rain).

4. Investigation of Winter Synoptic Events and Perspectives

From the absence of a significant diurnal cycle, the coherency between day-to-day variations recorded in vapor and precipitation isotopic measurements, as well as the similarity between data from stations at two different altitudes, we have demonstrated that the signal recorded at AWIPEV is dominated by day-to-day variability associated with synoptic weather. We can hence use surface vapor measurements to study large-scale processes in this sector and we concentrate in the following on the important winter variability of temperature, humidity, and water stable isotopes. Moreover, Rinke et al. (2017) and Zhang et al. (2004) have shown that the cyclone intensity and frequency are higher in winter which makes this season of particular interest for the Svalbard region.

4.1. Detection of Synoptic Events

We first characterize the signature of synoptic events on the vapor isotopic composition from our time series. Synoptic events are defined as events of a time scale of 1 to 5 days and a spatial scale of several hundred to several thousand kilometers. In the Arctic, increases of the humidity of 3,000 ppmv within a period of 2 days, following the criteria used by Bonne et al. (2014), are associated with synoptic events, particularly in winter when almost all events are linked to anomalies in temperature due to air masses coming from the North Atlantic (Nomokonova et al., 2020). We use these criteria to identify the humidity peaks from our time series in Svalbard and pinpoint synoptic events. During the period from 1 June 2014 to 1 June 2015 (Figure 5), these large and abrupt events provide 39% of the total precipitation amount (as identified using ERA5 total precipitation variable) and are associated with large peaks in the water vapor isotopic composition, that is, a systematic increase in $\delta^{18}O$ and in most cases a decrease in d-excess.

Over the full year period, we identify 16 such synoptic events numbered 14-1 to 14-9 and 14-A to 14-G: only three are detected during the warm plateau in summer (14-A, 14-B, and 14-C in Figure 5), two of them occurring at the very end of the summer period when temperature and humidity start to decrease (14-B and 14-C). The other 13 occur outside of this period. Winter climate variability is dominated by the moist events occurring 5 to 9 times between the months of November and March, which is consistent with the relatively high increase of vertically integrated water vapor content in the region in winter (Nomokonova et al., 2020; Rinke et al., 2019). In the following, we thus focus this study on the humidity peaks over the coldest period (i.e., temperature below 5°C, large predominance of snow precipitation) from 1 November to 31 March, hence events 14-1 to 14-9 in Figures 5 and 6. Moreover, such events are expected to be an important signal in the accumulated snow in the region which has a direct application for the interpretation of ice cores (Divine et al., 2008; Isaksson et al., 2005; Opel et al., 2009). These nine events, each one associated with a temperature increase larger than 7°C, systematically display an increase in $\delta^{18}O$ larger than 7‰ within 2 days. The d-excess generally shows a decreasing signal larger than 10‰ within 2 days (observed for all events except for 14-3).

The same detection routine (increase of more than 3,000 ppmv in 2 days) is then applied over the four winters (November to March) of our record, for years 2014 to 2018. In total, we detect 28 events (Figure 6 for winter 14, Figure S14 for following years). All of these humidity events display a significant increase of $\delta^{18}O$ (more than 7‰ in 2 days). A majority of these peaks seem associated with a decrease of d-excess.

4.2. Possible Mechanisms at Play

As mentioned in section 1, d-excess variations can be used to trace changes in moisture sources. We investigate here how the combination of surface vapor $\delta^{18}O$ and d-excess can provide information on the origin of the air mass trajectories coming to Svalbard during our winter humidity peaks. For this purpose, we calculate the correlation coefficient between the increase of $\delta^{18}O$ and the corresponding hourly variation of
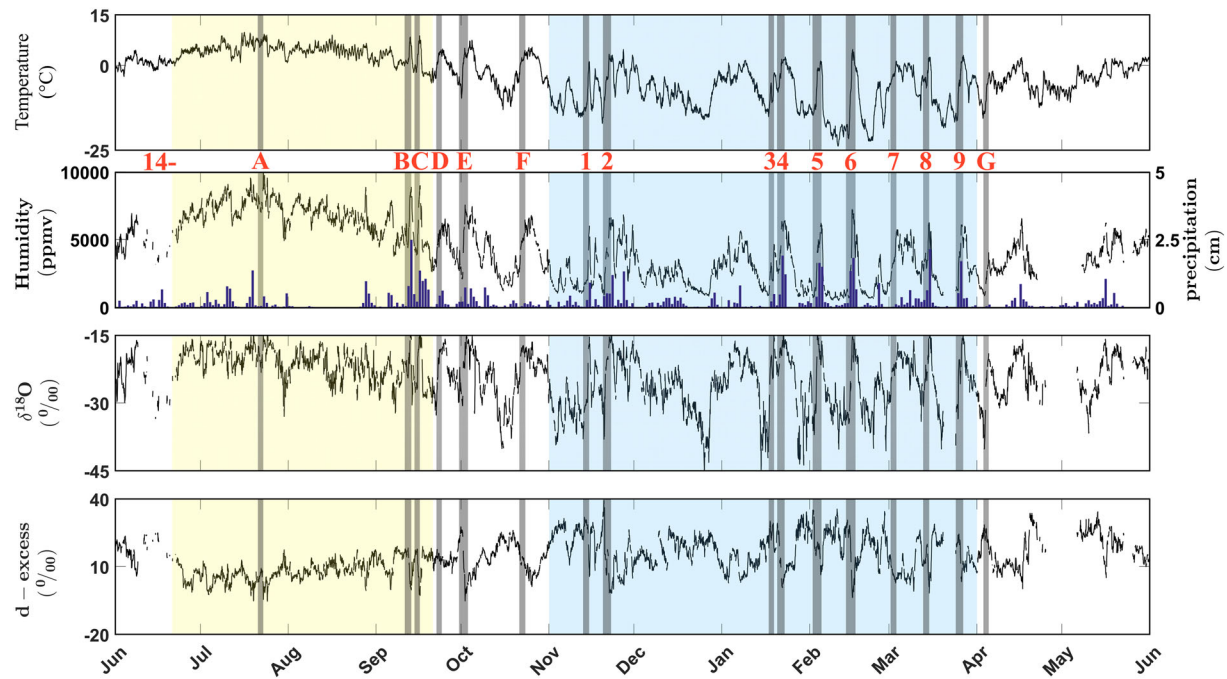
Figure 5. One-year data series (1 June 2014 to 1 June 2015) of measurements at AWIPEV station. Blue bars in the second panel stand for daily precipitation amount derived from ERA-5. In yellow: summer season, in blue: extended winter season (from November to March). Gray bars are humidity peaks defined as an increase of 3,000 ppmv (or more) within 2 days (numbered from 14-1 to 14-9 during extended winter, and from 14-A to 14-G out of this period).

d-excess over the two consecutive days of one identified humidity peak. We tag in green in Figures 6 and S14 the time periods with both (i) a significant increase in δ^{18}O (>7‰) and (ii) a significant anticorrelation between d-excess and δ^{18}O ($R < -0.7$).

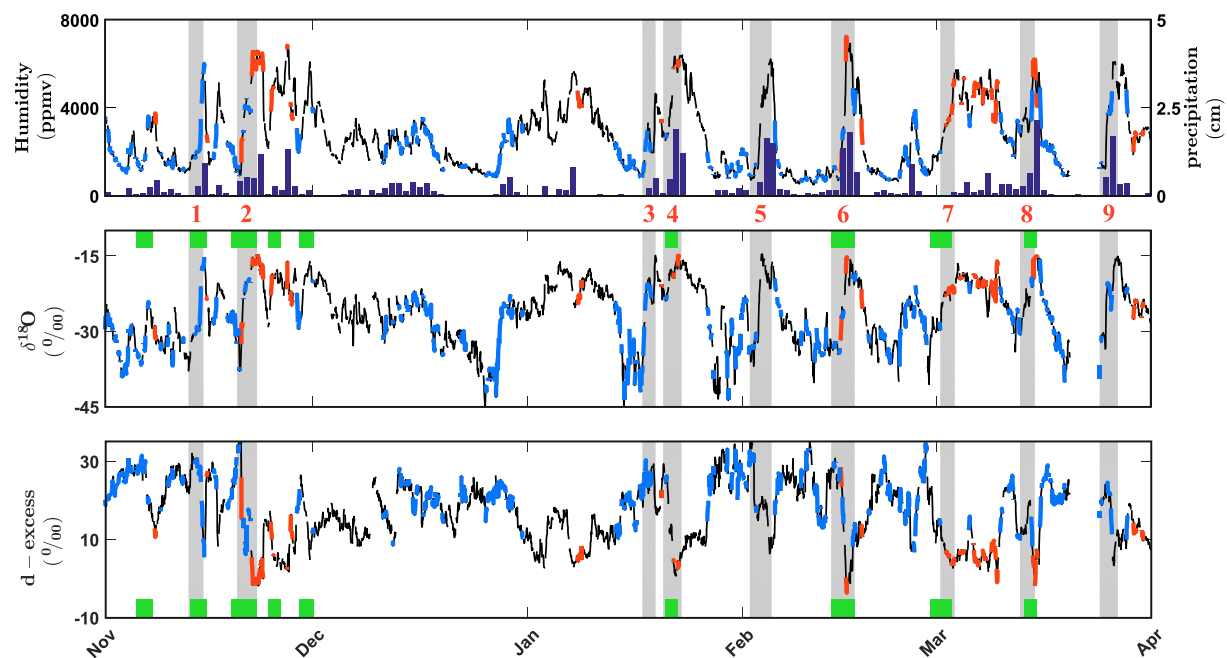**Figure 6.** Links between the water vapor isotopic composition and air mass origin over winter 14. Gray bars are humidity peaks as defined in the text. Red and blue lines correspond to air masses with specific source location (North Atlantic and Arctic respectively) estimated with Hysplit (see text). Time periods with particularly high anticorrelation ($R < -0.7$) between δ^{18}O and d-excess are highlighted by the green bars.

Several explanations can be proposed for the observed anticorrelation between d-excess and δ^{18}O over the highlighted green periods. A first effect can be linked to the role of precipitation and transport. A δ^{18}O versus d-excess anticorrelation can be obtained in the case of intense distillation as observed in the water vapor isotopic composition in continental polar regions after a long trajectory without significant recycling or high in the atmosphere (Risi et al., 2010; Touzeau et al., 2016). This effect could play a role in the polar Svalbard context and can best be evidenced using a logarithm definition of the d-excess (Dütsch et al., 2017; Uemura et al., 2012), see details in Text S2 and Figure S2. Still, the observed range of δ^{18}O values is rather high, ruling out a case of intense distillation. The other dominant effects are linked to evaporation and reevaporation which occur along the water mass trajectory. Because of kinetic effects, evaporation of water under relatively dry air conditions should lead to lower δ^{18}O and higher d-excess in vapor, based on the simple approach of Merlivat and Jouzel (1979) applied to several systems (e.g., Sodemann et al., 2017); this effect probably plays a role here. Then, as shown in Risi et al. (2008), reevaporation is one of the major processes explaining the isotopic signal in regions with strong local precipitation, characterized by the so-called amount effect (decrease in δ^{18}O and increase in d-excess for strong precipitation rate). Rain reevaporation leads to an increase of d-excess in the water vapor. However, this effect is dominant mostly in tropical regions or below clouds in case of dry air advection from the free troposphere. We are studying here moist events with a large proportion of snow precipitation so that rain reevaporation is probably not the main driver of our isotopic signal. Finally, another possible process is the sublimation of snow (Kopec et al., 2019; Pang et al., 2019). However, sublimation of snow is an effect that is only significant in the continental polar regions when moisture travels above the continental ice sheet, which differs from our coastal Svalbard context.

We thus conclude that the process explaining the largest part of the d-excess vs δ^{18}O relationship in the water vapor over Svalbard is most likely linked with a change in evaporative conditions in the moisture source region. In particular, low d-excess is generally associated with high relative humidity at evaporation because kinetic fractionation is reduced when the air is saturated with water vapor. Where relative humidity of the atmosphere is low, for instance, near the sea ice margins or during SLOE events (Strong Large-scale Ocean Evaporation), d-excess values in surface vapor are high (Kurita, 2003). This mechanism has already been proposed to explain high d-excess values observed in the Arctic region (Aemisegger, 2018; Aemisegger & Sjolte, 2018; Bonne et al., 2019; Steen-Larsen et al., 2015) and should also be considered to understand our records. Because of the probable influence of source evaporative conditions and distillation along the trajectory on the isotopic signal, we thus focus in the following on the role of changes in air mass trajectories and origin of air masses using back trajectories calculated for each wet winter (humidity peak) event.

4.3. Back Trajectories and Isotopic Signature

The Hysplit back trajectories were first clustered according to their origin: the back trajectories with their origin (first 2 days) within the Arctic sector (latitude higher than 80°N and longitude between 60°W and 60°E) are displayed in blue; the back trajectories with their origin within the Atlantic sector (latitudes below Iceland are displayed in red (Figures 6, 7, and S14).

When comparing the anticorrelation between δ^{18}O and d-excess with the air mass origin over Svalbard, we observe that in most of the cases, the synoptic events with strong δ^{18}O versus d-excess anticorrelation (14 events) are associated with an air mass origin located in the North Atlantic during the humidity peak (Table 2, 12 peaks over 14). For all these 14 events, air masses have an Arctic origin prior to the humidity increase. On the other hand, out of the 14 events with no clear anticorrelation detected, eight are related to different air mass source (Table 2) mainly from the Arctic sector (Greenland, Siberia, or Scandinavia). However, for six events (bold in the last column of Table 2), there is no clear anticorrelation between δ^{18}O and d-excess although air originates from the North Atlantic. We now illustrate in Figure 7 these different behaviors by focusing on four particular humidity peaks (16-5, 15-2, 17-1, 16-2) and complementing then by the Flexpart diagnostic (Text S9 and Figure S15).

The humidity peak 16-5 (Figure 7, first panel) has a water isotopic signal showing a clear anticorrelation between the abrupt increase in δ^{18}O (more than 9‰) and the abrupt decrease in d-excess (more than 10‰) over two consecutive days (1–3 February). In parallel, back trajectories shift rapidly (in less than 1 day) from a situation with air of Arctic origin to a situation with air of Atlantic origin. This example illustrates the general behavior observed for events marked in red on the fifth line in Table 2: an anticorrelation
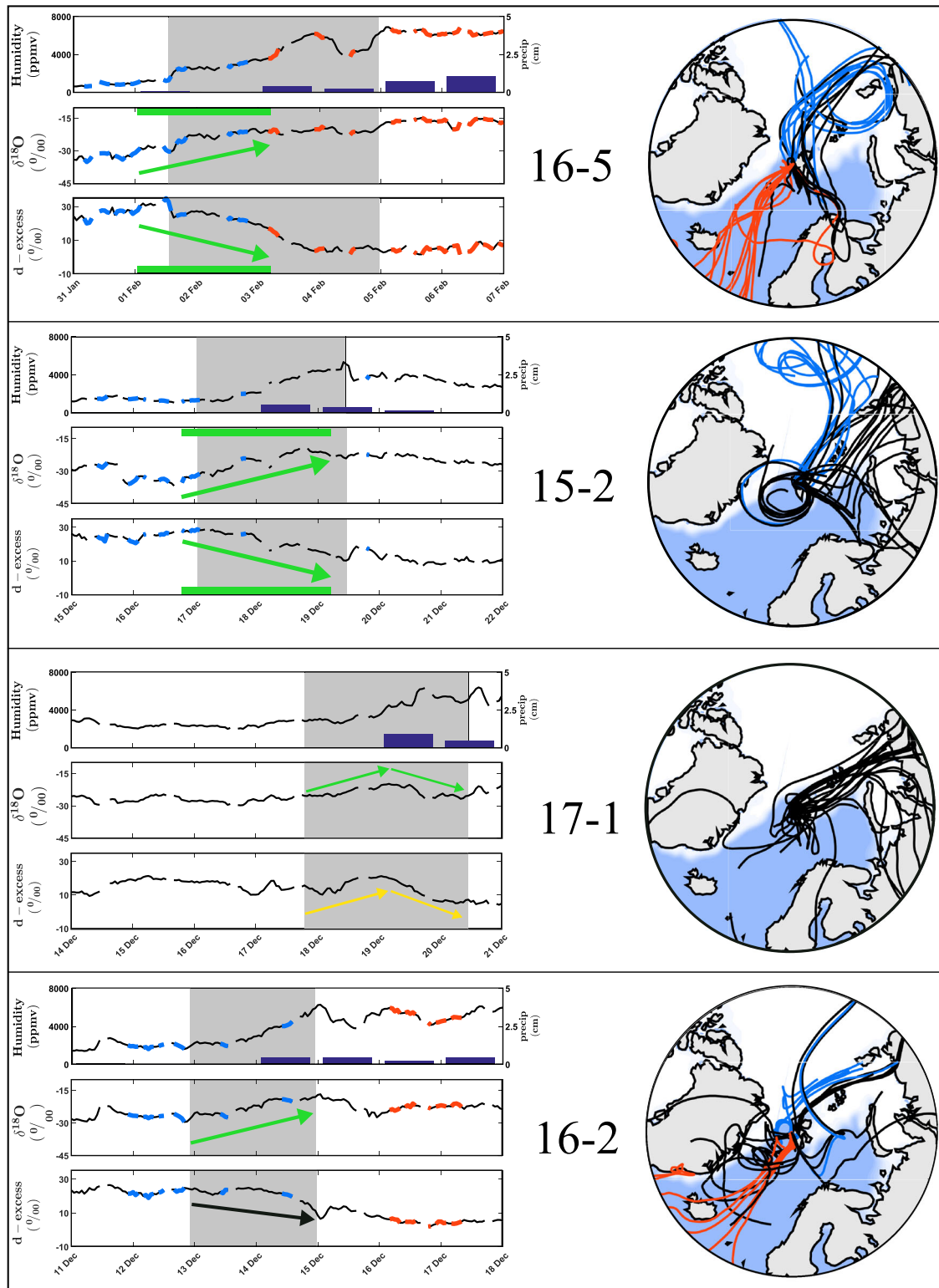
Figure 7. Examples of four humidity peaks (16-5, 15-2, 17-1, 16-2). The left panels display the humidity, precipitation, $\delta^{18}O$ and d-excess records over 7 days including the humidity peak event (in gray). The right panels display the associated 5 days back trajectories computed with Hysplit. On both panels, red lines are for air parcel originating from the North Atlantic sector (first 2 days over the 5 days of calculation), while blue lines stand for the Arctic sector. Black lines and black back trajectories are unlabeled. Arrows indicate the correlation between $\delta^{18}O$ and d-excess: Pairs of green arrows are for high anticorrelation, pairs of green and yellow arrows are for high correlation and a pair of green and black arrow stands for no specific correlation. Sea ice concentration is represented in white (calculated from ERA-5 reanalyses).

Table 2
Classification of Extended Winter Humidity Peaks (Figures 6 and S14)

Year					14								15							16					17			Tot
Humidity peaks number	1	2	3	4	5	6	7	8	9	1	2	3	4	5	6	7	1	2	3	4	5	6	7	1	2	3	4	5	28
Atlantic source		X		X		X	X	X					X	X	X	X		X		X	X	X	X		X	X	X	X	18
Other source	X		X		X				X	X	X	X					X		X					X					10
$(\delta^{18}O, \text{d-excess}): R < -0.7$	X	X		X		X	X	X			X		X	X		X				X	X		X			X			14
$(\delta^{18}O, \text{d-excess}): R > -0.7$			X		X				X	X		X			X		X	X	X			X		X	X		X	X	14

Note. "Atlantic source" means that humidity peaks are associated with North Atlantic air masses while "other source" mainly stands for Arctic origins. The last two lines separate events associated with a specific isotopic signature (high anticorrelation between $\delta^{18}O$ and d-excess: R < −0.7) from others (no high anticorrelation between $\delta^{18}O$ and d-excess or positive correlation). Red boxes: moist events associated with North Atlantic origins based on the Hysplit diagnostic. Blue boxes: moist events mainly associated with Arctic origins based on the Hysplit diagnostic. The specific isotopic signature (fifth line) is most of the times associated with North Atlantic origins (red boxes). On the fifth line (sixth line), blue boxes (red boxes) contradict the general interpretation. Gray boxes: events for which back trajectories are shown in Figure 7.

between the increase of $\delta^{18}O$ and the decrease of d-excess over winter humidity peak is the signature of a rapid shift of air origin from Arctic origin to oceanic midlatitude (Atlantic region). Flexpart footprints help us to refine the location of the air parcel origin and allow us to relate this characteristic isotopic signature to a shift to a source located in the North Atlantic Ocean at a latitude below 60°N (Figure S15).

For only two events out of the 14 events identified over the winters of our study (14-1 and 15-2), the anticorrelation between an increase in $\delta^{18}O$ and a decrease in d-excess is not associated with a shift of moisture origin toward the Atlantic Ocean (Table 2). During the event 15-2 (second panel of Figure 7), air origin shifts from the Arctic ocean covered by sea ice to open waters of Barents and Greenland seas. We propose that this strong change of air mass origin can lead to the observed isotopic signal. This shift in air mass origin is confirmed by additional footprints analyses performed using the Flexpart tool: A large fraction of Flexpart back trajectories show an origin of air mass in the atmospheric boundary layer above Arctic sea ice before the humidity peak to a local source, suggesting that the moisture increase results from local evaporation (Figure S15).

Fourteen events do not show any strong anticorrelation between $\delta^{18}O$ and d-excess (Table 2, last column). In a majority of cases (8 peaks over 14), the shift of air mass trajectories happens within the Northern sector (Arctic: Greenland, Siberia, or Scandinavia). This is the case of the humidity peak beginning on 16 December 2017 (event 17-1, third panel of Figure 7): the $\delta^{18}O$ increase (more than 12‰) and the following decrease (slightly less than to 8‰), are not anticorrelated with the d-excess signal. In fact, the d-excess is correlated with $\delta^{18}O$ ($R > 0.7$) during the abrupt increase in humidity. In parallel, the back trajectories display a change in the origin of air parcels within the Northern sector: from continental region of Siberia (14–18 December) to sea ice margin close to Svalbard (18–20 December). At the beginning of the event, relatively low d-excess could be explained by soil evaporation in the Siberian continental regions (Aemisegger et al., 2014). At the humidity maximum, the d-excess decrease can be explained by local oceanic evaporation in a moist atmosphere, hence under a small air-sea humidity gradient. The pattern of change in air mass origin is confirmed by the Flexpart footprints analysis (Figure S15, third panel).

For the other events (15-6, 16-2, 16-6, 17-2, 17-4, and 17-5) during which the change of air mass origin (from Arctic to North Atlantic origin) is not associated with d-excess versus $\delta^{18}O$ anticorrelation signature, the shift of air mass origin is either too slow or does not involve latitudes southern than 65°N to be imprinted in the water isotopes records as illustrated for event 16-2 in Figure 7 (fourth panel). This conclusion is strengthened by Flexpart footprints which show that the red back trajectories computed with Hysplit can be misleading: at the humidity maximum, most of the air masses originate in fact locally, from areas located at amplitudes higher than 70°N of the Greenland Sea (Figure S15, fourth panel). This explains why the isotopic signal is ambiguous over this particular event.

4.4. Implications

Our exceptionally long water vapor isotopic data set complements previous findings from records of isotopic composition of water vapor in the North Atlantic and Arctic regions. In particular, Bonne et al. (2015) also

identified synoptic events during autumn, winter, and spring associated with the same kind of humidity peaks (more than 3,000 ppmv increase in 2 days) in Greenland at the Ivittuut station. In their study, all identified humidity peaks display a strong anticorrelation between a δ^{18}O increase and a d-excess decrease and all events correspond to an arrival of moisture from the Atlantic Ocean, south of Greenland. Such a pattern agrees with our finding over the Svalbard region, that is, the anticorrelation between δ^{18}O and d-excess indicates a shift to Atlantic origin for the air masses during the cold season humidity peaks. However, such an isotopic signature for an Atlantic moisture origin has more implications in Svalbard since a significant proportion of air masses during humidity peaks does not come from the Atlantic, opposite to South Greenland where humidity peaks systematically originate from the Atlantic. Water isotopes bring thus a strong added value to identify shifts in Svalbard air mass origins.

Our results have implication for the interpretation of d-excess in the Arctic region. While, high d-excess values observed in the Arctic regions have been associated with moisture source in high-latitude regions covered by sea ice (Bonne et al., 2019; Kurita, 2003; Steen-Larsen et al., 2015), others suggest that a switch in moisture sources from low to high latitude should result in a decrease of d-excess (Kopec et al., 2019). Our study rather confirms the pattern where air masses coming from high latitude carry vapor with higher d-excess: in fact, the humidity peaks associated with air originating from the Arctic do not show any d-excess decrease, but rather an increase as observed during events 14-9, 16-3, 17-1, 17-2, 17-5 with relatively high d-excess values and positive correlation between δ^{18}O and d-excess.

First, the moist winter events are a significant source of precipitation over Svalbard. Our results also have implications to be further explored in ice core science and climate modeling. From the links made between vapor and precipitation measurements (section 3.4), their isotopic fingerprints archived in snow could help deciphering past changes in the origin of moisture coming to the Arctic region using Svalbard ice core records.

Second, Svalbard is a key location to look at the atmospheric circulation and transport of moist air at the boundary between north Atlantic and Arctic with a possible large influence of the sea ice. Isotopic composition of water vapor brings an important diagnostic on shift of air mass origin that should be combined with modeling approaches including water isotopes description. One of the largest limitations when dealing with isotope-enabled models is their inability to reproduce the large variations of d-excess in the north Atlantic and Arctic regions (Risi et al., 2010; Steen-Larsen et al., 2017; Werner et al., 2011). Part of this limitation may be linked to an inaccurate simulation of the water vapor isotopic composition in the boundary layer or during sublimation over the sea ice or over snow (Bonne et al., 2019; Kopec et al., 2019; Steen-Larsen et al., 2017; Werner et al., 2011). It may also be linked to an inaccurate transportation model of the atmospheric moisture (e.g., isotopic composition of water vapor is very sensitive to the model horizontal advection (Hendricks et al., 2000). Because Svalbard is at a key location with alternation of moisture arrival from Arctic and Atlantic, the comparison between our long water vapor isotopic record and atmospheric simulations may help disentangling the influence of marine boundary layer processes and atmospheric circulation.

Finally, our study focused on the large humidity peaks occurring during winter but there is a clear interest to look as well at the other circulation patterns during winter as well as other seasons with a possible larger influence of Arctic air masses. While the isotopic pattern is not as systematic as for the winter humidity peaks with North Atlantic origin, periods with moisture originating from the Arctic may be characterized by an opposite isotopic signature. However, Arctic air is often dry and calibration of water vapor isotopic record is still difficult at low humidity (below 2,000 ppmv) hence limiting such an application (Casado et al., 2016; Ritter et al., 2016). A new generation of laser spectroscopy instrument and associated calibration setup should soon permit to address such limitations. Our full data set is available (Zenodo repository) and we encourage and welcome its use for other studies focusing on arctic air intrusions as well as on more local processes, such as polar lows or local orographic effects of air flows in the fjord.

5. Conclusion

We presented the first continuous multiyear record of water isotopes in surface water vapor at Ny-Ålesund (Svalbard), a key location at the edge of the current Arctic sea ice winter extent. We have evidenced that this data set reflects the regional dynamics of the atmospheric water cycle. In this region, winter weather regime

is characterized by the recurrence of humid events lasting a few days. Combining $\delta^{18}O$ and d-excess in the water vapor with back trajectories, we identify the isotopic signature of a shift of air mass origin from the Arctic to the North Atlantic below 60°N through a positive peak of $\delta^{18}O$ anticorrelated with d-excess. The isotopic signature of moisture transported from an Arctic source is less unequivocal but is generally marked by positive peaks of both $\delta^{18}O$ and d-excess.

Here, we focused our analyses on winter wet events, but our record can also be used to further explore the relationships between surface water vapor and precipitation isotopic composition and changes in air mass origins or moisture evaporation conditions during other seasons and at the interannual scale. This could be achieved using not only air mass back trajectories as used here but also more sophisticated diagnoses of moisture transport and evaporation conditions (Papritz & Sodemann, 2018; Sodemann et al., 2008).

Data Availability Statement

The full data set archiving is underway and will be fully available through a Zenodo repository (https://doi.org/10.5281/zenodo.3689566). Until publication, the data set is with limited access.

References

Aemisegger, F. (2018). On the link between the North Atlantic storm track and precipitation deuterium excess in Reykjavik. *Atmospheric Science Letters*, *19*(12), e865. https://doi.org/10.1002/asl.865

Aemisegger, F., Pfahl, S., Sodemann, H., Lehner, I., Seneviratne, S. I., & Wernli, H. (2014). Deuterium excess as a proxy for continental moisture recycling and plant transpiration. *Atmospheric Chemistry and Physics*, *14*(8), 4029–4054. https://doi.org/10.5194/acp-14-4029-2014

Aemisegger, F., & Sjolte, J. (2018). A climatology of strong large-scale ocean evaporation events. Part II: Relevance for the deuterium excess signature of the evaporation flux. *Journal of Climate*, *31*(18), 7313–7336. https://doi.org/10.1175/JCLI-D-17-0592.1

Aemisegger, F., Sturm, P., Graf, P., Sodemann, H., Pfahl, S., Knohl, A., & Wernli, H. (2012). Measuring variations of $\delta^{18}O$ and δ^2H in atmospheric water vapour using two commercial laser-based spectrometers: An instrument characterisation study. *Atmospheric Measurement Techniques*, *5*(7), 1491–1511. https://doi.org/10.5194/amt-5-1491-2012

Alekseev, G., Kuzmina, S., Bobylev, L., Urazgildeeva, A., & Gnatiuk, N. (2019). Impact of atmospheric heat and moisture transport on the Arctic warming. *International Journal of Climatology*, *39*(8), 3582–3592. https://doi.org/10.1002/joc.6040

Angert, A., Cappa, C. D., & DePaolo, D. J. (2004). Kinetic ^{17}O effects in the hydrologic cycle: Indirect evidence and implications. *Geochimica et Cosmochimica Acta*, *68*(17), 3487–3495. https://doi.org/10.1016/j.gca.2004.02.010

Arctic Monitoring and Assessment Programme. (2017). *Snow, water, ice and permafrost in the Arctic (SWIPA) 2017* (pp. xiv +269). Oslo, Norway: Arctic Monitoring and Assessment Programme (AMAP).

Bailey, A., Noone, D., Berkelhammer, M., Steen-Larsen, H. C., & Sato, P. (2015). The stability and calibration of water vapor isotope ratio measurements during long-term deployments. *Atmospheric Measurement Techniques*, *8*(10), 4521–4538. https://doi.org/10.5194/amt-8-4521-2015

Bastrikov, V., Steen-Larsen, H. C., Masson-Delmotte, V., Gribanov, K., Cattani, O., Jouzel, J., & Zakharov, V. (2014). Continuous measurements of atmospheric water vapour isotopes in western Siberia (Kourovka). *Atmospheric Measurement Techniques*, *7*(6), 1763–1776. https://doi.org/10.5194/amt-7-1763-2014

Benetti, M., Lacour, J. -L., Sveinbjörnsdóttir, A. E., Aloisi, G., Reverdin, G., Risi, C., et al. (2018). A framework to study mixing processes in the marine boundary layer using water vapor isotope measurements. *Geophysical Research Letters*, *45*, 2524–2532. https://doi.org/10.1002/2018GL077167

Benetti, M., Steen-Larsen, H. C., Reverdin, G., Sveinbjörnsdóttir, Á. E., Aloisi, G., Berkelhammer, M. B., et al. (2017). Stable isotopes in the atmospheric marine boundary layer water vapour over the Atlantic Ocean, 2012–2015. *Scientific Data*, *4*(1), 160128. https://doi.org/10.1038/sdata.2016.128

Berkelhammer, M., Noone, D. C., Steen-Larsen, H. C., Bailey, A., Cox, C. J., O'Neill, M. S., et al. (2016). Surface-atmosphere decoupling limits accumulation at summit, Greenland. *Science Advances*, *2*(4), e1501704. https://doi.org/10.1126/sciadv.1501704

Bintanja, R., & Selten, F. M. (2014). Future increases in Arctic precipitation linked to local evaporation and sea-ice retreat. *Nature*, *509*(7501), 479–482. https://doi.org/10.1038/nature13259

Bonne, J.-L., Behrens, M., Meyer, H., Kipfstuhl, S., Rabe, B., Schönicke, L., et al. (2019). Resolving the controls of water vapour isotopes in the Atlantic sector. *Nature Communications*, *10*(1), 1632. https://doi.org/10.1038/s41467-019-09242-6

Bonne, J.-L., Masson-Delmotte, V., Cattani, O., Delmotte, M., Risi, C., Sodemann, H., & Steen-Larsen, H. C. (2014). The isotopic composition of water vapour and precipitation in Ivittuut, southern Greenland. *Atmospheric Chemistry and Physics*, *14*(9), 4419–4439. https://doi.org/10.5194/acp-14-4419-2014

Bonne, J.-L., Steen-Larsen, H. C., Risi, C., Werner, M., Sodemann, H., Lacour, J.-L., et al. (2015). The summer 2012 Greenland heat wave: In situ and remote sensing observations of water vapor isotopic composition during an atmospheric river event. *Journal of Geophysical Research: Atmospheres*, *120*, 2970–2989. https://doi.org/10.1002/2014JD022602

Bréant, C., Leroy-Dos Santos, C., Agosta, C., Casado, M., Fourré, E., Goursaud, S., et al. (2019). Coastal water vapor isotopic composition driven by katabatic wind variability in summer at Dumont d'Urville, coastal East Antarctica. *Earth and Planetary Science Letters*, *514*, 37–47. https://doi.org/10.1016/j.epsl.2019.03.004

Casado, M., Landais, A., Masson-Delmotte, V., Genthon, C., Kerstel, E., Kassi, S., et al. (2016). Continuous measurements of isotopic composition of water vapour on the EastAntarctic plateau. *Atmospheric Chemistry and Physics*, *16*(13), 8521–8538. https://doi.org/10.5194/acp-16-8521-2016

Ciais, P., & Jouzel, J. (1994). Deuterium and oxygen 18 in precipitation: Isotopic model, including mixed cloud processes. *Journal of Geophysical Research*, *99*(D8), 16793. https://doi.org/10.1029/94JD00412

Craig, H., & Gordon, L. I. (1965). Deuterium and oxygen 18 variations in the ocean and the marine atmosphere. In *Stable isotopes in oceanographic studies and paleotemperatures*. Spoleto, Italy.

Dahlke, S., Hughes, N. E., Wagner, P. M., Gerland, S., Wawrzyniak, T., Ivanov, B., & Maturilli, M. (2020). The observed recent surface air temperature development across Svalbard and concurring footprints in local sea ice cover. *International Journal of Climatology*, *40*. https://doi.org/10.1002/joc.6517

Dahlke, S., & Maturilli, M. (2017). Contribution of atmospheric advection to the amplified winter warming in the Arctic North Atlantic region. *Advances in Meteorology*, *2017*, 1–8. https://doi.org/10.1155/2017/4928620

Dansgaard, W. (1964). Stable isotopes in precipitation. *Tellus*, *16*(4), 436–468. https://doi.org/10.1111/j.2153-3490.1964.tb00181.x

Ding, Q., Schweiger, A., L'Heureux, M., Battisti, D. S., Po-Chedley, S., Johnson, N. C., et al. (2017). Influence of high-latitude atmospheric circulation changes on summertime Arctic sea ice. *Nature Climate Change*, *7*(4), 289–295. https://doi.org/10.1038/nclimate3241

Divine, D. V., Isaksson, E., Pohjola, V., Meijer, H., van de Wal, R. S. W., Martma, T., et al. (2008). Deuterium excess record from a small Arctic ice cap. *Journal of Geophysical Research*, *113*, D19104. https://doi.org/10.1029/2008JD010076

Dufour, A., Zolina, O., & Gulev, S. K. (2016). Atmospheric moisture transport to the Arctic: Assessment of reanalyses and analysis of transport components. *Journal of Climate*, *29*(14), 5061–5081. https://doi.org/10.1175/JCLI-D-15-0559.1

Dütsch, M., Pfahl, S., & Sodemann, H. (2017). The impact of nonequilibrium and equilibrium fractionation on two different deuterium excess definitions. *Journal of Geophysical Research: Atmospheres*, *122*, 12–732. https://doi.org/10.1002/2017JD027085

Eckhardt, S., Hermansen, O., Grythe, H., Fiebig, M., Stebel, K., Cassiani, M., et al. (2013). The influence of cruise ship emissions on air pollution in Svalbard—A harbinger of a more polluted Arctic? *Atmospheric Chemistry and Physics*, *13*(16), 8401–8409. https://doi.org/10.5194/acp-13-8401-2013

Galewsky, J., Steen-Larsen, H. C., Field, R. D., Worden, J., Risi, C., & Schneider, M. (2016). Stable isotopes in atmospheric water vapor and applications to the hydrologic cycle: Isotopes in the atmospheric water cycle. *Reviews of Geophysics*, *54*, 809–865. https://doi.org/10.1002/2015RG000512

Gat, J. R. (1996). Oxygen and hydrogen isotopes in the hydrologic cycle. *Annual Review of Earth and Planetary Sciences*, *24*(1), 225–262. https://doi.org/10.1146/annurev.earth.24.1.225

Gjelten, H. M., Nordli, Ø., Isaksen, K., Førland, E. J., Sviashchennikov, P. N., Wyszynski, P., et al. (2016). Air temperature variations and gradients along the coast and fjords of western Spitsbergen. *Polar Research*, *35*(1), 29878. https://doi.org/10.3402/polar.v35.29878

Goosse, H., Kay, J. E., Armour, K. C., Bodas-Salcedo, A., Chepfer, H., Docquier, D., et al. (2018). Quantifying climate feedbacks in polar regions. *Nature Communications*, *9*(1), 1919. https://doi.org/10.1038/s41467-018-04173-0

Hanssen-Bauer, I., & Førland, E. (1998). Long-term trends in precipitation and temperature in the Norwegian Arctic: Can they be explained by changes in atmospheric circulation patterns? *Climate Research*, *10*, 143–153. https://doi.org/10.3354/cr010143

Hao, M., Luo, Y., Lin, Y., Zhao, Z., Wang, L., & Huang, J. (2019). Contribution of atmospheric moisture transport to winter Arctic warming. *International Journal of Climatology*, *39*(5), 2697–2710. https://doi.org/10.1002/joc.5982

Hendricks, M. B., DePaolo, D. J., & Cohen, R. C. (2000). Space and time variation δ^{18}O and δD in precipitation: Can paleotemperature be estimated from ice cores? *Global Biogeochemical Cycles*, *14*(3), 851–861. https://doi.org/10.1029/1999GB001198

Picarro Inc. (2009). *L1102-i analyzer user's guide*. Sunnyvale, CA, USA: Picarro Inc. Retrieved from https://www.picarro.com/support/documents

Picarro Inc. (2016). *L2130-i analyzer user's guide*. Sunnyvale, CA, USA: Picarro Inc. Retrieved from https://www.picarro.com/support/documents

International Atomic Energy Agency. (2006). *Reference sheet for international measurement standards*. International Atomic Energy Agency (IAEA). Retrieved from https://nucleus.iaea.org/rpst/documents/VSMOW_SLAP.pdf

Isaksen, K., Nordli, Ø., Førland, E. J., Łupikasza, E., Eastwood, S., & Niedźwiedź, T. (2016). Recent warming on Spitsbergen-influence of atmospheric circulation and sea ice cover. *Journal of Geophysical Research: Atmospheres*, *121*, 11,913–11,931. https://doi.org/10.1002/2016JD025606

Isaksson, E., Kohler, J., Pohjola, V., Moore, J., Igarashi, M., Karlöf, L., et al. (2005). Two ice-core δ^{18}O records from Svalbard illustrating climate and sea-ice variability over the last 400 years. *The Holocene*, *15*(4), 501–509. https://doi.org/10.1191/0959683605hl820rp

Jouzel, J. (2003). Water stable isotopes: Atmospheric composition and applications in polar ice core studies. *Treatise on Geochemistry*, *4*, 213–243. https://doi.org/10.1016/B0-08-043751-6/04040-8

Jouzel, J., Delaygue, G., Landais, A., Masson-Delmotte, V., Risi, C., & Vimeux, F. (2013). Water isotopes as tools to document oceanic sources of precipitation: Water isotopes and precipitation origin. *Water Resources Research*, *49*, 7469–7486. https://doi.org/10.1002/2013WR013508

Jouzel, J., & Merlivat, L. (1984). Deuterium and oxygen 18 in precipitation: Modeling of the isotopic effects during snow formation. *Journal of Geophysical Research*, *89*(D7), 11749–11,757. https://doi.org/10.1029/JD089iD07p11749

Kopec, B. G., Feng, X., Posmentier, E. S., & Sonder, L. J. (2019). Seasonal deuterium excess variations of precipitation at summit, Greenland, and their climatological significance. *Journal of Geophysical Research: Atmospheres*, *124*, 72–91. https://doi.org/10.1029/2018JD028750

Kopec, B. G., Lauder, A. M., Posmentier, E. S., & Feng, X. (2014). The diel cycle of water vapor in West Greenland: West Greenland diel cycle of water vapor. *Journal of Geophysical Research: Atmospheres*, *119*, 9386–9399. https://doi.org/10.1002/2014JD021859

Kurita, N. (2003). Relationship between the variation of isotopic ratios and the source of summer precipitation in eastern Siberia. *Journal of Geophysical Research*, *108*(D11), 4339. https://doi.org/10.1029/2001JD001359

Liu, C., & Barnes, E. A. (2015). Extreme moisture transport into the Arctic linked to Rossby wave breaking: Extreme moisture flux and wave breaking. *Journal of Geophysical Research: Atmospheres*, *120*, 3774–3788. https://doi.org/10.1002/2014JD022796

Majoube, M. (1971). Fractionnement en δ^{18}O entre la glace et la vapeur d'eau. *Journal de Chimie Physique*, *68*, 625–636. https://doi.org/10.1051/jcp/1971680625

Masson-Delmotte, V., Hou, S., Ekaykin, A., Jouzel, J., Aristarain, A., Bernardo, R. T., et al. (2008). A review of Antarctic surface snow isotopic composition: Observations, atmospheric circulation, and isotopic modeling. *Journal of Climate*, *21*(13), 3359–3387. https://doi.org/10.1175/2007JCLI2139.1

Maturilli, M. (2018). High resolution radiosonde measurements from station Ny-Ålesund (2017-12). *PANGAEA*. https://doi.org/10.1594/PANGAEA.886871

Maturilli, M. (2020a). Basic and other measurements of radiation at station Ny-Ålesund (2020-04). *PANGAEA*. https://doi.org/10.1594/PANGAEA.917580

Maturilli, M. (2020b). High resolution radiosonde measurements from station Ny-Ålesund (2017-04 et seq). *PANGAEA*. https://doi.org/10.1594/PANGAEA.914973

Maturilli, M., & Ebell, K. (2018). Twenty-five years of cloud base height measurements by ceilometer in Ny-Ålesund, Svalbard. *Earth System Science Data*, *10*(3), 1451–1456. https://doi.org/10.5194/essd-10-1451-2018

Maturilli, M., & Kayser, M. (2017). Arctic warming, moisture increase and circulation changes observed in the Ny-Ålesund homogenized radiosonde record. *Theoretical and Applied Climatology*, *130*(1–2), 1–17. https://doi.org/10.1007/s00704-016-1864-0

Meredith, M., Sommerkorn, M., Cassota, S., Derksen, C., Ekaykin, A., & Hollowed, A. (2019). *IPCC special report on the ocean and cryosphere in a changing climate: Chapter 3: Polar regions*.

Merlivat, L., & Nief, G. (1967). Fractionnement isotopique lors des changements d'état solide-vapeur et liquide-vapeur de l'eau à des températures inférieures à 0°C. *Tellus*, *19*(1), 122–127. https://doi.org/10.1111/j.2153-3490.1967.tb01465.x

Merlivat, L., & Jouzel, J. (1979). Global climatic interpretation of the deuterium-oxygen 18 relationship for precipitation. *Journal of Geophysical Research*, *84*(C8), 5029. https://doi.org/10.1029/JC084iC08p05029

Naakka, T., Nygård, T., Vihma, T., Sedlar, J., & Graversen, R. (2019). Atmospheric moisture transport between mid-latitudes and the Arctic: Regional, seasonal and vertical distributions. *International Journal of Climatology*, *39*(6), 2862–2879. https://doi.org/10.1002/joc.5988

Ngan, F., Loughner, C. P., & Stein, A. (2019). The evaluation of mixing methods in HYSPLIT using measurements from controlled tracer experiments. *Atmospheric Environment*, *219*, 117043. https://doi.org/10.1016/j.atmosenv.2019.117043

Nomokonova, T., Ebell, K., Löhnert, U., Maturilli, M., & Ritter, C. (2020). The influence of water vapor anomalies on clouds and their radiative effect at Ny-Ålesund. *Atmospheric Chemistry and Physics*, *20*(8), 5157–5173. https://doi.org/10.5194/acp-20-5157-2020

Opel, T., Fritzsche, D., Meyer, H., Schütt, R., Weiler, K., Ruth, U., et al. (2009). 115 year ice-core data from Akademii Nauk ice cap, Severnaya Zemlya: High-resolution record of Eurasian Arctic climate change. *Journal of Glaciology*, *55*(189), 21–31. https://doi.org/10.3189/002214309788608029

Overland, J. E., & Wang, M. (2018). Arctic-midlatitude weather linkages in North America. *Polar Science*, *16*, 1–9. https://doi.org/10.1016/j.polar.2018.02.001

Pang, H., Hou, S., Landais, A., Masson-Delmotte, V., Jouzel, J., Steen-Larsen, H. C., et al. (2019). Influence of summer sublimation on δD, δ^{18}O, and δ^{17}O in precipitation, East Antarctica, and implications for climate reconstruction from ice cores. *Journal of Geophysical Research: Atmospheres*. https://doi.org/10.1029/2018JD030218

Papritz, L., & Sodemann, H. (2018). Characterizing the local and intense water cycle during a cold air outbreak in the Nordic seas. *Monthly Weather Review*, *146*(11), 3567–3588. https://doi.org/10.1175/MWR-D-18-0172.1

Rayleigh, L. (1902). LIX. On the distillation of binary mixtures. *The London, Edinburgh, and Dublin Philosophical Magazine and Journal of Science*, *4*(23), 521–537. https://doi.org/10.1080/14786440209462876

Rinke, A., Maturilli, M., Graham, R. M., Matthes, H., Handorf, D., Cohen, L., et al. (2017). Extreme cyclone events in the Arctic: Wintertime variability and trends. *Environmental Research Letters*, *12*(9), 094006. https://doi.org/10.1088/1748-9326/aa7def

Rinke, A., Segger, B., Crewell, S., Maturilli, M., Naakka, T., Nygård, T., et al. (2019). Trends of vertically integrated water vapor over the Arctic during 1979–2016: Consistent moistening all over? *Journal of Climate*, *32*(18), 6097–6116. https://doi.org/10.1175/JCLI-D-19-0092.1

Risi, C., Bony, S., & Vimeux, F. (2008). Influence of convective processes on the isotopic composition (δ^{18}O and δD) of precipitation and water vapor in the tropics: 2. Physical interpretation of the amount effect. *Journal of Geophysical Research*, *113*, D19306. https://doi.org/10.1029/2008JD009943

Risi, C., Bony, S., Vimeux, F., & Jouzel, J. (2010). Water-stable isotopes in the LMDZ4 general circulation model: Model evaluation for present-day and past climates and applications to climatic interpretations of tropical isotopic records. *Journal of Geophysical Research*, *115*, D12118. https://doi.org/10.1029/2009JD013255

Ritter, F., Steen-Larsen, H. C., Werner, M., Masson-Delmotte, V., Orsi, A., Behrens, M., et al. (2016). Isotopic exchange on the diurnal scale between near-surface snow and lower atmospheric water vapor at Kohnen station, East Antarctica. *The Cryosphere*, *10*(4), 1647–1663. https://doi.org/10.5194/tc-10-1647-2016

Screen, J. A., & Simmonds, I. (2010). The central role of diminishing sea ice in recent Arctic temperature amplification. *Nature*, *464*(7293), 1334–1337. https://doi.org/10.1038/nature09051

Smith, R. B., & Evans, J. P. (2007). Orographic precipitation and water vapor fractionation over the southern Andes. *Journal of Hydrometeorology*, *8*(1), 3–19. https://doi.org/10.1175/JHM555.1

Sodemann, H., Schwierz, C., & Wernli, H. (2008). Interannual variability of Greenland winter precipitation sources: Lagrangian moisture diagnostic and North Atlantic oscillation influence. *Journal of Geophysical Research*, *113*, D03107. https://doi.org/10.1029/2007JD008503

Sodemann, H., Aemisegger, F., Pfahl, S., Bitter, M., Corsmeier, U., Feuerle, T., et al. (2017). The stable isotopic composition of water vapour above Corsica during the HyMeX SOP1 campaign: Insight into vertical mixing processes from lower-tropospheric survey flights. *Atmospheric Chemistry and Physics*, *17*(9), 6125–6151. https://doi.org/10.5194/acp-17-6125-2017

Steen-Larsen, H. C., Johnsen, S. J., Masson-Delmotte, V., Stenni, B., Risi, C., Sodemann, H., et al. (2013). Continuous monitoring of summer surface water vapor isotopic composition above the Greenland ice sheet. *Atmospheric Chemistry and Physics*, *13*(9), 4815–4828. https://doi.org/10.5194/acp-13-4815-2013

Steen-Larsen, H. C., Masson-Delmotte, V., Hirabayashi, M., Winkler, R., Satow, K., Prié, F., et al. (2014). What controls the isotopic composition of Greenland surface snow? *Climate of the Past*, *10*(1), 377–392. https://doi.org/10.5194/cp-10-377-2014

Steen-Larsen, H. C., Masson-Delmotte, V., Sjolte, J., Johnsen, S. J., Vinther, B. M., Bréon, F.-M., et al. (2011). Understanding the climatic signal in the water stable isotope records from the NEEM shallow firn/ice cores in Northwest Greenland. *Journal of Geophysical Research*, *116*(D6), D06108. https://doi.org/10.1029/2010JD014311

Steen-Larsen, H. C., Risi, C., Werner, M., Yoshimura, K., & Masson-Delmotte, V. (2017). Evaluating the skills of isotope-enabled general circulation models against in situ atmospheric water vapor isotope observations: Evaluating isotope-enabled GCMs. *Journal of Geophysical Research: Atmospheres*, *122*, 246–263. https://doi.org/10.1002/2016JD025443

Steen-Larsen, H. C., Sveinbjörnsdottir, A. E., Jonsson, T., Ritter, F., Bonne, J.-L., Masson-Delmotte, V., et al. (2015). Moisture sources and synoptic to seasonal variability of North Atlantic water vapor isotopic composition: North Atlantic water vapor isotopes. *Journal of Geophysical Research: Atmospheres*, *120*, 5757–5774. https://doi.org/10.1002/2015JD023234

Stein, A. F., Draxler, R. R., Rolph, G. D., Stunder, B. J. B., Cohen, M. D., & Ngan, F. (2015). NOAA's HYSPLIT atmospheric transport and dispersion modeling system. *Bulletin of the American Meteorological Society*, *96*(12), 2059–2077. https://doi.org/10.1175/BAMS-D-14-00110.1

Stern, L. A., & Blisniuk, P. M. (2002). Stable isotope composition of precipitation across the southern Patagonian Andes: Stable isotope composition of precipitation. *Journal of Geophysical Research*, *107*(D23), 4667. https://doi.org/10.1029/2002JD002509

Stohl, A., Forster, C., Frank, A., Seibert, P., & Wotawa, G. (2005). The Lagrangian particle dispersion model FLEXPART version 6.2. *Atmospheric Chemistry and Physics*, *5*. https://doi.org/10.5194/acp-5-2461-2005

Touzeau, A., Landais, A., Stenni, B., Uemura, R., Fukui, K., Fujita, S., et al. (2016). Acquisition of isotopic composition for surface snow in East Antarctica and the links to climatic parameters. *The Cryosphere*, *17*. https://doi.org/10.5194/tc-10-837-2016

Tremoy, G., Vimeux, F., Cattani, O., Mayaki, S., Souley, I., & Favreau, G. (2011). Measurements of water vapor isotope ratios with wavelength-scanned cavity ring-down spectroscopy technology: New insights and important caveats for deuterium excess measurements in tropical areas in comparison with isotope-ratio mass spectrometry: Measuring tropical water vapor isotope ratios using WS-CRDS. *Rapid Communications in Mass Spectrometry*, *25*(23), 3469–3480. https://doi.org/10.1002/rcm.5252

Uemura, R., Masson-Delmotte, V., Jouzel, J., Landais, A., Motoyama, H., & Stenni, B. (2012). Ranges of moisture-source temperature estimated from Antarctic ice cores stable isotope records over glacial–interglacial cycles. *Climate of the Past*, *8*(3), 1109–1125. https://doi.org/10.5194/cp-8-1109-2012

Vázquez, M., Nieto, R., Drumond, A., & Gimeno, L. (2016). Moisture transport into the Arctic: Source-receptor relationships and the roles of atmospheric circulation and evaporation. *Journal of Geophysical Research: Atmospheres*, *121*, 13,493–13,509. https://doi.org/10.1002/2016JD025400

Walsh, J. E., Fetterer, F., Scott stewart, J., & Chapman, W. L. (2017). A database for depicting Arctic Sea ice variations back to 1850. *Geographical Review*, *107*(1), 89–107. https://doi.org/10.1111/j.1931-0846.2016.12195.x

Werner, M., Langebroek, P. M., Carlsen, T., Herold, M., & Lohmann, G. (2011). Stable water isotopes in the ECHAM5 general circulation model: Toward high-resolution isotope modeling on a global scale. *Journal of Geophysical Research*, *116*, D15109. https://doi.org/10.1029/2011JD015681

Woods, C., Caballero, R., & Svensson, G. (2013). Large-scale circulation associated with moisture intrusions into the Arctic during winter. *Geophysical Research Letters*, *40*, 4717–4721. https://doi.org/10.1002/grl.50912

Zhang, X., Walsh, J. E., & Zhang, J. (2004). Climatology and interannual variability of Arctic cyclone activity: 1948–2002. *Journal of Climate*, *17*, 19. https://doi.org/10.1175/1520-0442(2004)017<2300:caivoa>2.0.co;2